After-pulsing and cross-talk comparison for KETEK PM1125NS-SB0, Hamamatsu S10362-11-100C and Hamamatsu S13360-3050CS.

1 Abstract

Silicon photomultipliers (SiPMs) have become extensive used recently. They exceed photomultiplier tubes on quantum efficiency, size and resistance to the magnetic field. However, due to the features of the structure they have a greater value of dark noise rate, as well as they have additional sources of noise: cross-talk and after-pulsing. In addition, these parameters may have a temperature dependence.

In this article we present results of a evaluation dark noise rate, probabilities of cross-talk and after-pulses at different voltages and temperatures for two modern SiPM: Hamamatsu S13360-3050CS and KETEK PM1125NS-SB0 and Hamamatsu S10362-11-100C SiPM from the previous generation. An offline signal processing was performed by a pulse approximation with reconstruction of amplitudes and start times to find these parameters. As a result, we found that at achieved measurement accuracy the dark noise rate has a temperature and a voltage dependence, but cross-talk and after-pulses probabilities have only the latter.

The measured cross-talk probabilities for KETEK PM1125NS-SB0 and Hamamatsu S13360-3050CS at their optimal operating voltage is about 6%, it is two times smaller than that for Hamamatsu S10362-11-100C. The fast component of after-pulses probability for KETEK PM1125NS-SB0 and Hamamatsu S13360-3050CS is about 12%, which is also almost 2 times smaller than sum of fast and slow components of after-pulses probability for Hamamatsu S10362-11-100C. The dark noise rate for Hamamatsu S13360-3050CS at 20 $^{\circ}C$ is only 30 kHz/mm^2 in comparison with 80 kHz/mm^2 for KETEK PM1125NS-SB0.

2 Introduction

For many years BINP has been developing the X-ray inspection systems [1]. These installations can be used in various fields: inspection at airports, subways or at work-places. Multistrip ionization chamber filled with pure Xe at 15 bar have been used as X-ray detector until now. However, this detector has a disadvantage - it works in charge integrating mode, so at low input flow of particles electronic noise seriously degrades quality of images. Another drawback is the insufficiently high detection efficiency of high-energy photons. In this regard, it was decided to choose a new detector based on a SiPM and a scintillator which may has higher detection efficiency and will operate in the direct photon counting mode.

The main purpose of this work was to measure after-pulses and cross-talk probabilities for two SiPMs: KETEK PM1125NS-SB0 and Hamamatsu S13360-3050CS and compare them with the characteristics of Hamamatsu S10362-11-100C - the device from the previous generation.

3 Measurement of breakdown voltage

One of the important characteristics of any SiPM is a breakdown voltage.

In many works it was shown that SiPM gain is a linear function of both a temperature and a voltage. Thus, the expression for gain $G(V,T)$ is written as follows: [2–5]:

$$G(V,T) = a \cdot V + b \cdot T + c \tag{1}$$

It is easy to find a breakdown voltage equating the gain from Eq.(1) to zero :

$$V_{BD}(T) = \frac{-(b \cdot T + c)}{a} = \frac{dV}{dT} \cdot T + const \tag{2}$$

In measurements an voltage error ΔV was estimated at 0.01 V, and a temperature error ΔT was estimated as the minimum temperature step 1 K divided by $\sqrt{12}$.

4 Cross-talk and after-pulses probabilities finding algorithm

4.1 Background

There are several algorithms for finding cross-talk probabilities. One of them is to measure a dark noise rate at different thresholds [6]. A cross-talk probability can be defined as the ratio of the rates with 1.5 photoelectrons(phe) and 0.5 photoelectrons threshold:

$$P_{X-talk} = \nu_{1.5phe}/\nu_{0.5phe} \tag{3}$$

However, this method has the significant disadvantage: after-pulses are indistinguishable from cross-talk if the former above a threshold. Furthermore, this algorithm does not use information about a signal shape. It makes a dependence on the threshold more blurred and makes a finding of the $\nu_{1.5pe}$ value more complicated.

An advanced algorithm should use an information about a waveform. There are two approaches for a signal processing: deconvolution [7] and an approximation with known waveform [8–10]. In our work we decided to use the method of signal approximation.

In the process of approximation we obtain amplitudes and time stamps of event. Using this information we recover the time constants and probabilities for after-pulses.

After-pulsing is retriggering of a cell originating from a capture of electrons into traps during an avalanche and their subsequent release in a time interval from a few nanoseconds to several microseconds [6]. After initial triggering a voltage in a cell decreases to a breakdown voltage and then will recover to its original value exponentially.

There are several processes, which may cause of a cell retriggering. The first is after-pulsing. Because of different physical reasons, there are two types of after-pulses: fast and slow [8–10]. The second is a cell retriggering could be induced by thermal generated electrons. Each of the processes have exponential distribution in time with its time constant τ:

$$f(\Delta t) = \frac{1}{\tau} \cdot \exp(-\Delta t/\tau), \tag{4}$$

Measuring distribution distances between the pulses it is possible to characterize the time constants and the probabilities of processes leading to the triggering.

If we consider only one exponential process, probability $P(t)$ that in the interval from 0 to t the pulse does not exist and in the interval from t to $t + \delta t$ one pulse occurs is given by $P_{exp}(t) = \nu \cdot e^{-t \cdot \nu} \cdot \delta t$, where ν - frequency of events for given process. For more complicated case when dark pulses or one type of after-pulses are taken into account the required probability $P(t)$ can be written as follows:

$$\begin{aligned} P(t) = P\{\text{there are not after-pulses from 0 to } t + \delta t\} \cdot \\ P\{\text{there is dark pulse from } t \text{ to } t + \delta t\} + \\ P\{\text{there is after-pulse from } t \text{ to } t + \delta t\} \cdot \\ P\{\text{there are not dark pulses from 0 to } t + \delta t\} \end{aligned} \tag{5}$$

The contribution of each process is as follows:

$$\begin{aligned} P\{\text{there are not after-pulses from 0 to } t + \delta t\} = (1 - p) + p \cdot e^{-\nu \cdot t} \\ P\{\text{there is dark pulse from } t \text{ to } t + \delta t\} = (\nu_{dc} \cdot e^{-\nu_{dc} \cdot t}) \cdot \delta t \\ P\{\text{there is after-pulse from } t \text{ to } t + \delta t\} = p \cdot (\nu \cdot e^{-\nu \cdot t}) \cdot \delta t \\ P\{\text{there are not dark pulses from 0 to } t + \delta t\} = e^{-\nu_{dc} \cdot t} \end{aligned} \tag{6}$$

Thus, substituting probabilities in Eq.(5) from Eq.(6) and reducing the resulting expression on δt we obtain the probability density of pulse intervals:

$$f(t) = p \cdot (\nu + \nu_{dc}) \cdot e^{-(\nu + \nu_{dc}) \cdot t} + (1 - p) \cdot \nu_{dc} \cdot e^{-\nu_{dc} \cdot t}, \tag{7}$$

where p - probability of after-pulses. It is worth noting that a similar formula is given in [10], but with a typo in the sign between the terms.

As a result, taking into account the fast and slow components of after-pulses and dark noise events the probability density distribution of pulse intervals can be written as follows:

$$\begin{aligned} f(t) = p_s \cdot p_f \cdot (\nu_s + \nu_f + \nu_{dc}) \cdot e^{-(\nu_s+\nu_f+\nu_{dc})\cdot t} + \\ p_s \cdot (1-p_f) \cdot (\nu_s + \nu_{dc}) \cdot e^{-(\nu_s+\nu_{dc})\cdot t} + \\ p_f \cdot (1-p_s) \cdot (\nu_f + \nu_{dc}) \cdot e^{-(\nu_f+\nu_{dc})\cdot t} + \\ (1-p_s) \cdot (1-p_f) \cdot \nu_{dc} \cdot e^{-\nu_{dc}\cdot t} \end{aligned} \tag{8}$$

Eq.(8) is valid if one measure the distance between the signals caused by the triggering of a single cell. Signals caused by the simultaneous triggering of two or more cells (because of cross-talk) shall be excluded from contribution.

In the article [9] it's shown another result for the probability density of pulse intervals which differ from presented here. This is due to the consideration of one more process - delayed cross-talk. However, in practice the probability of delayed cross-talk is much lower than the probability of direct cross-talk, and in our experiments we did not observe it. The information about other processes that are responsible for a cell triggering can be found in [11].

4.2 Signal finder

Schematic overview of the experimental setup for recording SiPM signals is shown in Fig.1.

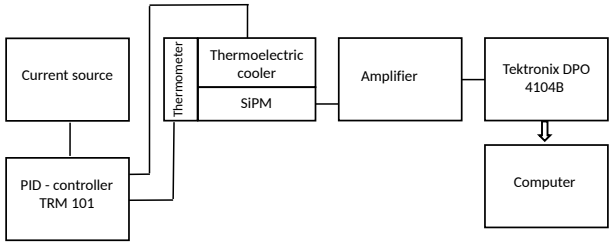

Fig. 1: Schematic overview of the experimental setup for recording SiPM signals.

Raw data were recorded with Tektronix oscilloscope DPO 4104B with sample rate 5GHz and length 5M sample. For each voltage and temperature combination 1000 files were recorded (total length is one second).

The signal can be presented as a sum of single-electron pulses $Signal_{1e}(t)$ with amplitude A_i and start time t_i:

$$V(t) = \sum_{i=0}^{N} A_i \cdot Signal_{1e}(t - t_i) + V_0, \tag{9}$$

where V_0 is baseline level.

The waveform of the single-electron pulse was found from analysis of the recorded signal and was approximated by an analytical function. The signal was processed by an algorithm that recover single-electron pulses without after-pulses impurities and averaged them. The waveform samples of the single-electron pulses for different SiPMs are shown in Fig.2. The waveforms were measured at different overvoltages and temperatures (from -8 to 27 $^{\circ}C$), but one remained practically unchanged.

Further, single-electron pulses were approximated by a function obtained from the convolution of Eq.(10) with the Gauss distribution describing a contribution of a limited operating speed of electronics. The final expression is shown in Eq.(11).

$$V(t) = A \cdot \exp\left[-\frac{t-t_0}{\tau_{rec}}\right] \cdot \left(1 - \exp\left[-\frac{t-t_0}{\tau_{rise}}\right]\right) \cdot \theta(t-t_0) + V_0, \tag{10}$$

$$V_{conv}(t) = V_0 + \frac{A}{2} \cdot \left(\{F(\sigma, \tau_{rec}) - F(\sigma, \tau_{total})\} \right), \text{ where} \tag{11}$$

$$F(\sigma, \tau) = \exp\left[\frac{\sigma^2 - 2t \cdot \tau}{2\tau^2}\right] \cdot \left(1 + Erf\left[\frac{t - \sigma^2/\tau}{\sigma\sqrt{2}}\right]\right),$$

$$\tau_{total} = \frac{\tau_{rec} \cdot \tau_{rise}}{\tau_{rec} + \tau_{rise}}$$

where A - a pulse amplitude, t_0 - a time delay, τ_{rec} - a recovery time of a cell, τ_{rise} - a rise time of a rising edge, V_0 - an offset, $\theta(t-t_0)$ - the Heaviside step function, σ - the standard deviation of the Gauss distribution.

The main task was to find A_i, t_i parameters of individual pulses. We can approximate a continuous waveform with 5MSamples length with Eq.(9) and $N \sim 30 \div 300$, but this task requires a huge amount of computing power. A continuous waveform were divided to practically independent fragments with $N = 1$ or $N = 2$ for the most parts.

The main problem with a processing is a noise. There are a lot of digital filters that can smooth a signal, but their use will lead to a loss of the information about after-pulses. After-pulses are exponentially distributed in time and with a high probability they occur at short times, when a cell has not yet recovered.

An accuracy of signals location can be improved if we transmit into the peak finder algorithm initial parameters close to true ones. For this purpose a signal derivative was calculated with the simultaneous smoothing (Savitsky-Golay third-order filter with the number of points equal to 51 (10.2 ns)) Thus, the information about the derivative was also involved in the processing.

To split a recorded file into multiple independent fragments, we used the following algorithm:

1) The first derivative was calculated using the Savitsky-Golay filter.

2) If a derivative and an amplitude were higher of the threshold values th_{der} and th_{amp}^{start} then the time 20 ns before this event with t_{trig} time was taken as start time t_{start} of a signal. This condition was necessary for the proper calculation of a baseline of the signal.
3) If after t_{trig} time more than $\tau_{amp}^{dead} = 5ns$ passed and the signal level was below the threshold amplitude th_{amp}^{stop} and ahead on 20 ns the derivative was below the threshold th_{der}, then this time was the end time of the signal. The amplitude threshold th_{amp}^{stop} was chosen as the intersection of the signal with the baseline.

To determine th_{amp}^{start} a dependence of events number versus the threshold voltage at different values of the dead time τ_{amp}^{dead} was measured. The examples of dependencies are shown in Fig. 4 for Hamamatsu S10362-11-100C at $T = 295K$ and $\Delta V = 1V$. The thresholds were practically independent of the selected dead time τ_{amp}^{dead}. The threshold for a triggering by amplitude th_{amp}^{start} was chosen at 1/2 amplitude of the single-electron signal (approximately $20mV$).

A similar graph can be drawn for the derivative (Fig. 5). We selected only those signals that exceed the amplitude threshold $th_{amp}^{stop} = 2mV$, because without this condition the distribution would be significantly distorted. Above the threshold value $4 \cdot 10^{-4} V/s$ the contribution of noise is significantly suppressed. This value was selected as th_{der}. Thresholds th_{der} and th_{amp}^{start} should be recalculated for other overvoltages.

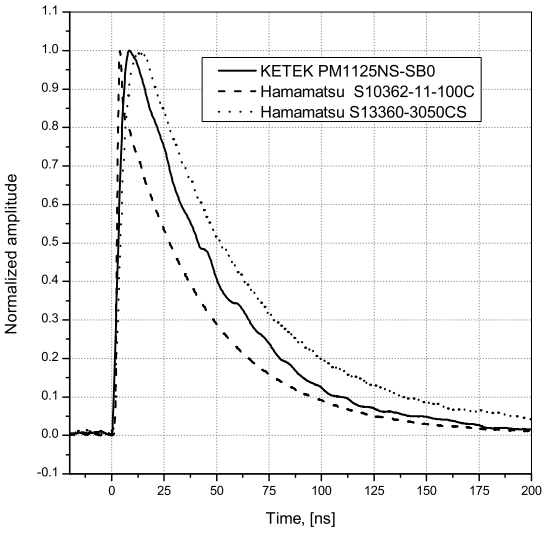

Fig. 2: The waveform of the single-electron pulse from different SiPMs.

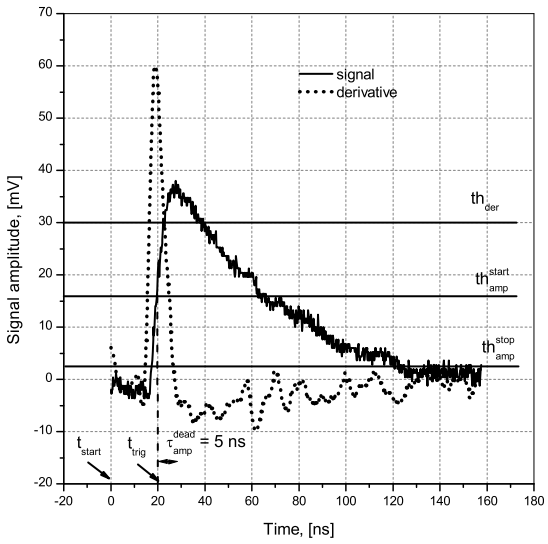

Fig. 3: The dependence of a signal amplitude and signal derivative versus time.

After this data processing the data files were divided into multiple independent fragments. At each part had to either one pulse or superposition of pulses.

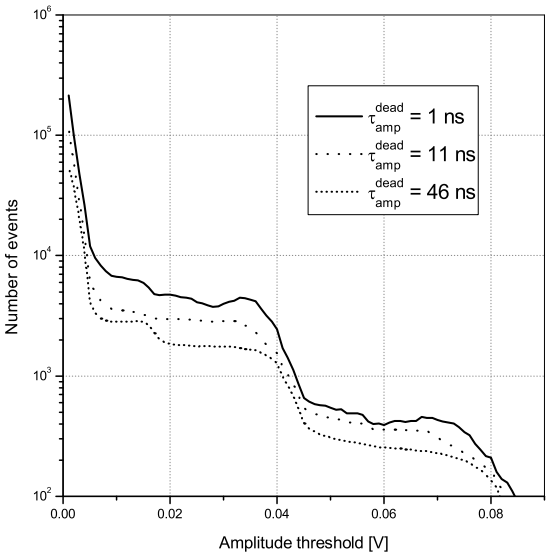

Fig. 4: The dependence of the number of found signals versus amplitude threshold and the dead time τ_{amp}^{dead} (Hamamatsu S10362-11-100C at 1V overvoltage and 295K

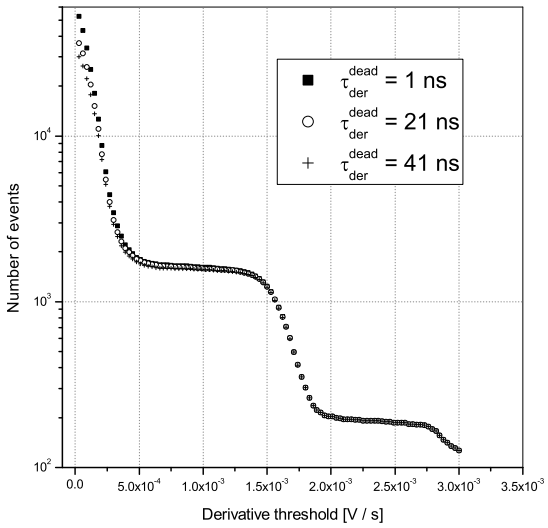

Fig. 5: The dependence of the number of found signals versus derivative threshold and the dead time τ_{der}^{dead} (Hamamatsu S10362-11-100C at 1V overvoltage and 295K). Only signals exceeding the threshold $th_{amp}^{stop} = 2mV/s$ were selected.

4.3 Correlation analysis

To find parameters A_i and t_i each fragment of waveform should be approximated with Eq.(9). This function internally nonlinear on t_i parameter therefore to get correct approximation it is necessary to set the initial value of parameter t_i close to the ones. To do this, we define $t_i^{initial}$ as the time when the 1st derivative reaches the maximum on the interval from the moment when the signal exceed the threshold th_{der} to this moment plus 5 ns: $t_i^{initial} = argmax(f'(t))$.

Further, an each independent fragment was approximated by Eq.(9) at $N = 1$. In Fig. 6 the correlation between the amplitude and χ^2/Dof is presented. One can notice a few outlying clusters: A_1, B_1, C_1 etc. The cluster A_1 corresponds to single-electron signals. Clusters B_1, C_1 etc. corresponds to events when simultaneously triggered two, three or more cells (cross-talk), and these signals clearly separated. Other events with the $\chi^2/Dof > 4$ value (we denote them as Z_1 cluster) correspond to the overlapped pulses(N > 1), located at a relatively short distance each other.

In the next step the events from the Z_1 cluster were approximated by Eq.(9) at $N = 2$. In that case, each event is characterized by four parameters: χ^2/Dof, amp_1 and amp_2 - amplitudes of the first and the second signals, Δt - a distance between the signals. In Fig. 7 a correlation between the total amplitude $amp_1 + amp_2$ and a

χ^2/Dof is presented.

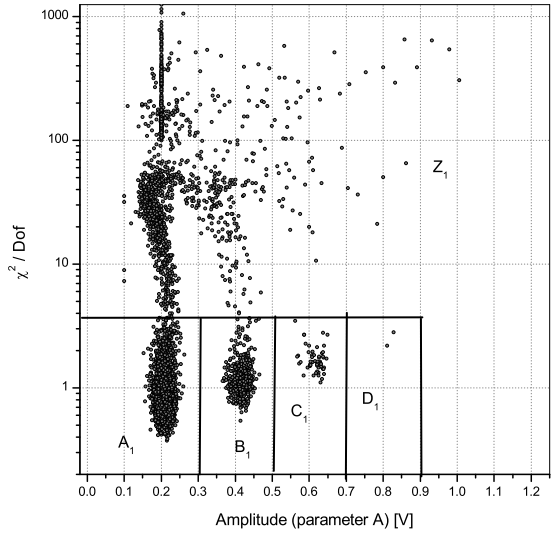

Fig. 6: The dependence of χ^2/Dof from the total amplitude $amp_1 + amp_2$ when approximating all pulses by one-component function (Hamamatsu S10362-11-100C at 1V overvoltage and 295K).

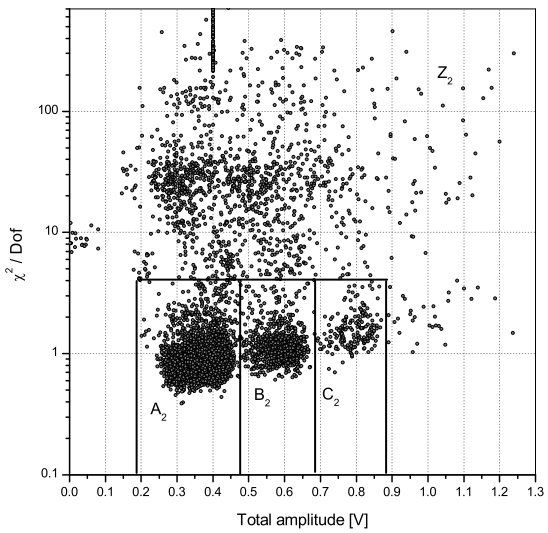

Fig. 7: The dependence of χ^2/Dof from the total amplitude $amp_1 + amp_2$ when approximating the Z_1 cluster (see Fig. 6) by two-component function (Hamamatsu S10362-11-100C at 1V overvoltage and 295K).

In this case there are several similar clusters: A_2, B_2, C_2 etc also. A more detailed information about the signals that forms these clusters can be obtained from the dependens $amp_1 + amp_2$ versus Δt calculated for clusters (Fig. 8 and Fig. 9).

The A_2 cluster consists of signals that are conventionally divided into two sets: α_1 и β_1. The set α_1 corresponds to the signals when the total amplitude equal to double amplitude of the single-electron pulse. This means that these signals were caused by triggering of separate cells and they could be treated as coincidence of dark noise events. At the same time signals from the set β_1 have an amplitude that depends on the distance between pulses. This means that the first signal was a single-electron pulse and the subsequent signal was an after-pulse. The similar correlation can be constructed for the B_2 set (Fig. 9). In this case, the set α_2 consists of two closely spaced signals one of which has 1e signal amplitude and another signal has the 2e amplitude caused by the simultaneous triggering of two cells due to cross-talk.

The set β_2 contains signals that can be divided into two groups. The first group was formed by signals in which two cells triggered simultaneously and then one of cells generated an after-pulse. The second group was formed by signals in which one cell triggered and then after-pulse occurred simultaneous with cross-talk. Large signals amplitude correspond to the events with a greater number of simultaneously triggered

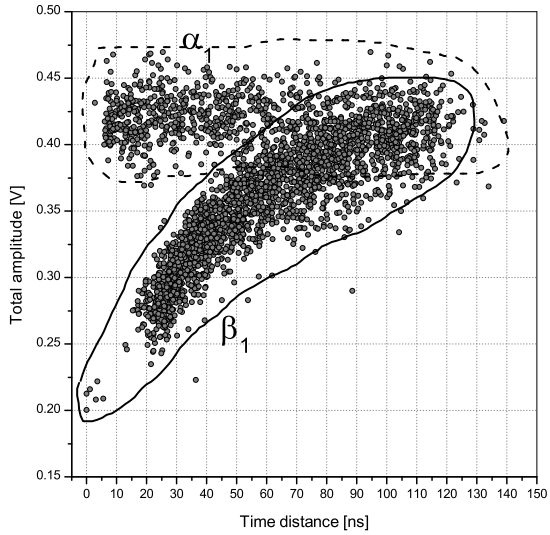

Fig. 8: The dependence of the total amplitude from the pulse interval when approximating the A_2 cluster (see Fig. 7) by two-component function (Hamamatsu S10362-11-100C at 1V overvoltage and 295K).

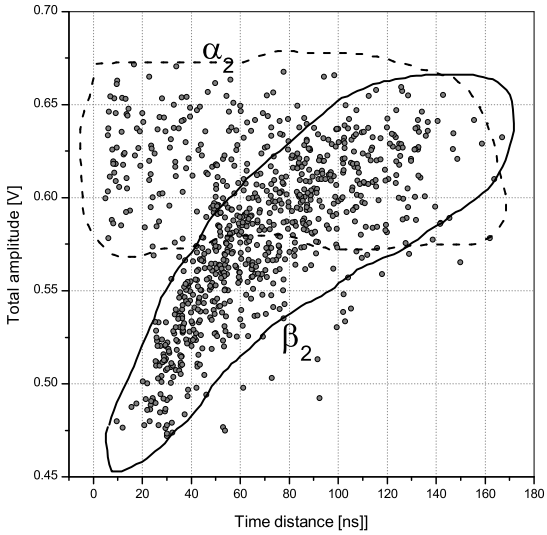

Fig. 9: The dependence of the total amplitude from the pulse interval when approximating the B_2 cluster (see Fig. 7) by two-component function (Hamamatsu S10362-11-100C at 1V overvoltage and 295K).

cells.

To built spectrum of intervals, we took into account only the pulses without cross-talk, i.e. we measured the distance between the pulses that belong to the A_1 or A_2 clusters. In the first approximation we can neglect events in the A_3, A_4 etc. clusters because of their relative small number.

The spectrum of intervals is shown in Fig. 10. By approximating the spectrum with Eq.(8) we can find p_s, p_f, ν_s, ν_f, ν_{DC} parameters. For the approximation RooFit package and unbinned fit were used.

As you can see there is a lack of events when the pulse interval less than 25 ns. The main reason for this is that the after-pulse occurs with the pulse interval less than 25 ns after the previous pulse, its amplitude is too small and this pulse cannot be reliable separated from noise. For the correct approximation we took into account only intervals that exceed a certain minimal value. Selection of the minimal interval effect on a value of component τ_f as could be seen in Fig. 11. For this type of SiMP at 295K temperature and 1V overvoltage 25 ns threshold was chosen. Further with a reducing the overvoltage the pulse interval threshold increases.

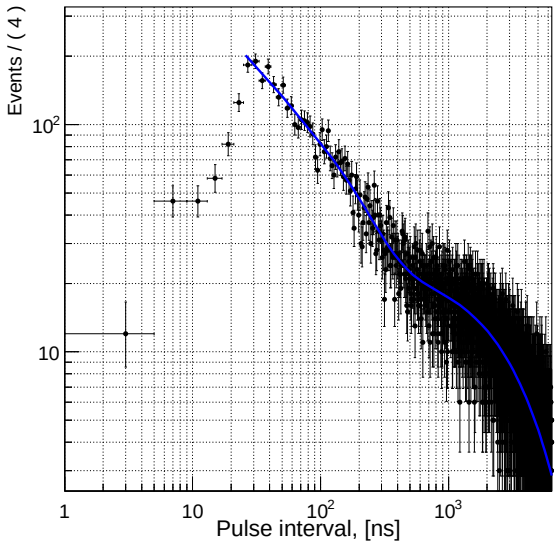

Fig. 10: The pulse interval spectrum approximated with Eq.(8) (Hamamatsu S10362-11-100C at 1V overvoltage and 295K).

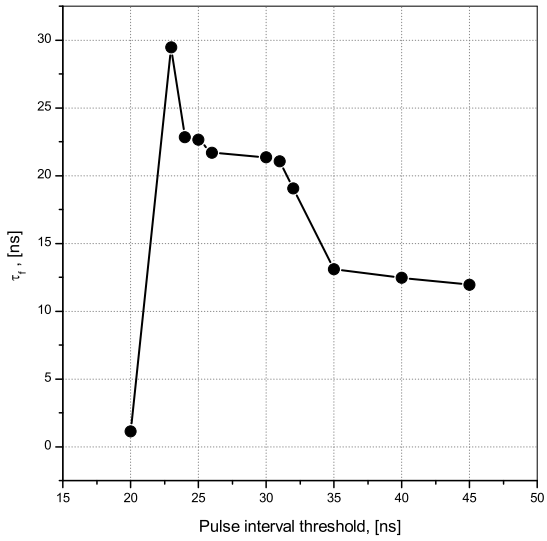

Fig. 11: The dependence of the afterpulse fast component from the pulse interval threshold. (Hamamatsu S10362-11-100C at 1V overvoltage and 295K).

5 Results and discussions

5.1 Dark noise rate

In Fig.12 the dependence of dark noise rate on a temperature is presented. This dependence is expressed by the following equation [4]:

$$\nu(\Delta V = const, T) = A(V) \cdot T^{3/2} \cdot \exp\left[-\frac{E_g}{2k_B \cdot T}\right], \tag{12}$$

where A is a constant, depending on voltage and technology, T is an absolute temperature, E_g is a bandgap, k_B is the Boltzmann constant.

In Fig.13, 14 the dependencies of dark noise rate on an overvoltage are presented. This dependence was approximated with linear law.

For Hamamatsu S13360-3050CS we were failed to collect enough statistics for data approximation in this manner because of its low noise level. In Fig.15 the dependence of dark noise rate on an overvoltage approximated with constant is presented. For the same reason, only limited data set at 290K(the maximum noise level) was obtained for KETEK PM1125NS-SB0.

5.2 Cross-talk probability

The A_1 cluster (Fig. 6) consists of single-electron pulses. The B_1 cluster consists of pulses caused by the simultaneous triggering of two cells. The C_1 cluster consists of

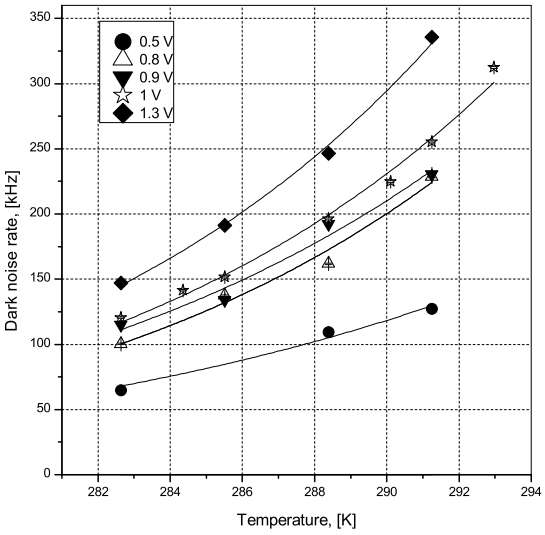

Fig. 12: The dependence of dark noise rate versus temperature at a fixed overvoltage (Hamamatsu S10362-11-100C).

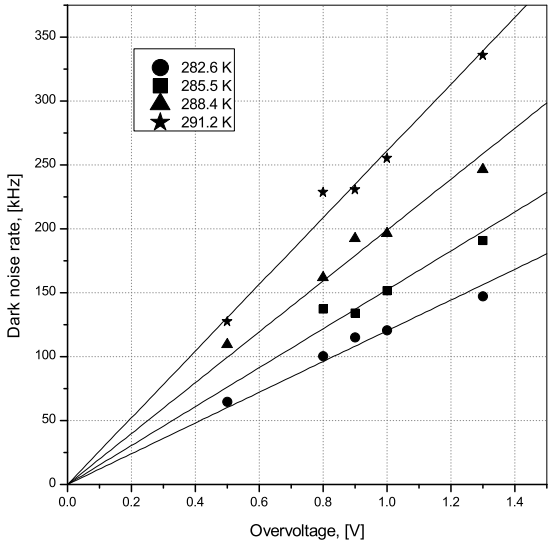

Fig. 13: The dependence of dark noise rate versus overvoltage at a fixed temperature (Hamamatsu S10362-11-100C).

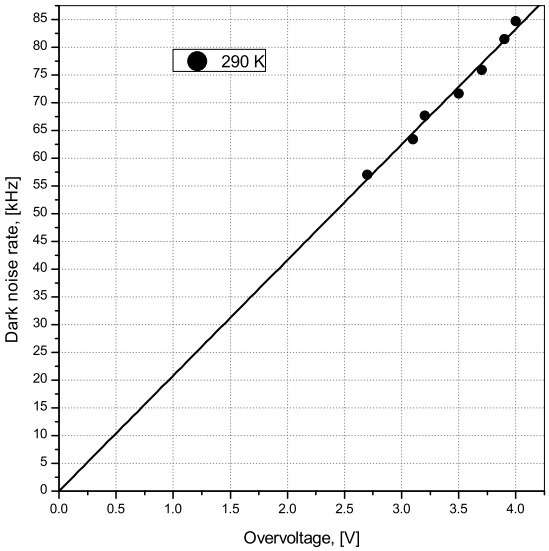

Fig. 14: The dependence of dark noise rate versus overvoltage at a fixed temperature (KETEK PM1125NS-SB0).

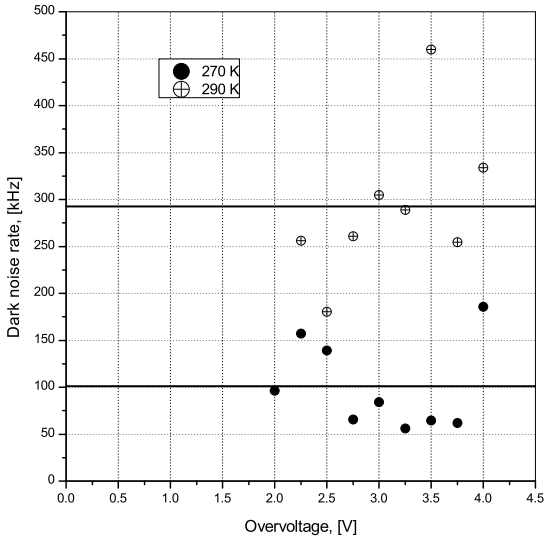

Fig. 15: The dependence of dark noise rate versus overvoltage at a fixed temperature (Hamamatsu S13360-3050CS).

pulses caused by the simultaneous triggering of three cells.

We calculate the cross-talk probability as follows:

$$P_{X-talk} = (N_{B_1} + N_{C_1})/(N_{A_1} + N_{B_1} + N_{C_1}) \tag{13}$$

This is an approximation because one should take into account the fact that a small

part of cross-talk events is contained in B_2, C_2, B_3, C_3, etc. clusters.

The cross-talk probability have the quadratic dependence of an overvoltage. This is explained by fact the cross-talk probability P_{x-talk} is proportional to the number of electrons in the avalanche G and the triggering probability of cells ε_{Geiger}. G and ε_{Geiger} have a linear dependence on an overvoltage(for ε_{Geiger} value the dependence differs from linear at a high overvoltage [12]):

$$P_{x-talk}(\Delta V) \propto G(\Delta V) \cdot \varepsilon_{Geiger}(\Delta V) \tag{14}$$

In Fig.17, 18, 19 the dependencies of cross-talk probability versus overvoltage approximated with a quadratic dependence are presented. In Fig.16 the dependence of cross-talk probability versus temperature is presented.

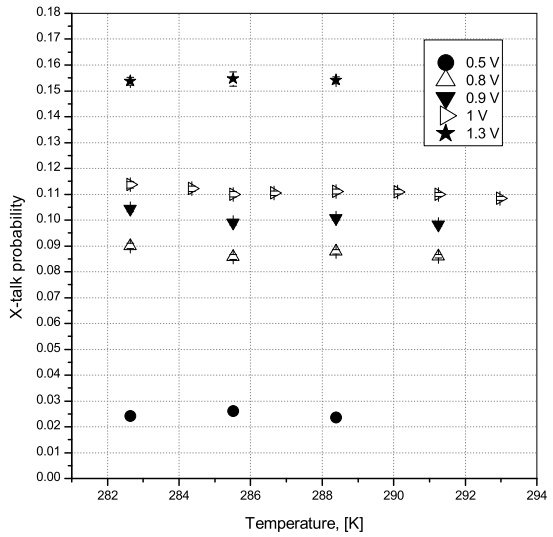

Fig. 16: The dependence of the cross-talk probability versus temperature at a fixed overvoltage (Hamamatsu S10362-11-100C).

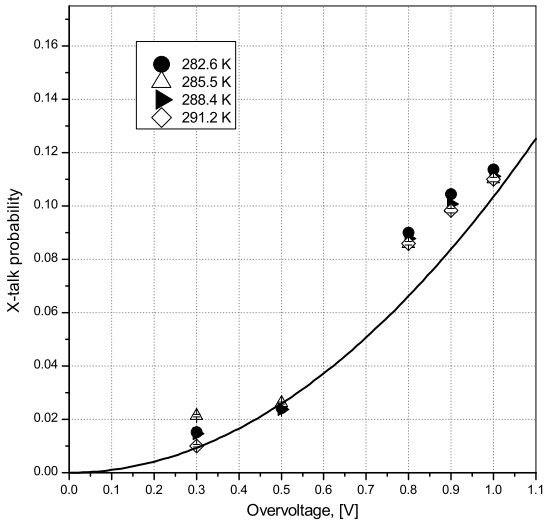

Fig. 17: The dependence of the cross-talk probability versus overvoltage at a fixed temperature (Hamamatsu S10362-11-100C).

Based on the experimental data, it can be concluded that the cross-talk probability is temperature independent.

5.3 Verification of the model of four nearest neighbors

In the model of four nearest neighbors it is assumed that a trigged cell can cause the triggering of only four nearest cells [7]. In this case, the cross-talk probability in the nearest cell p is related to the full cross-talk probability P_{x-talk} by the equation:

$$(1-p)^4 = 1 - P_{X-talk} \tag{15}$$

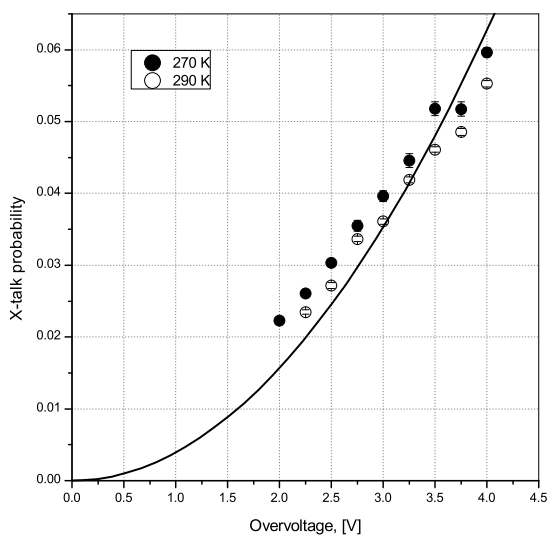

Fig. 18: The dependence of the cross-talk probability versus overvoltage at a fixed temperature (Hamamatsu S13360-3050CS).

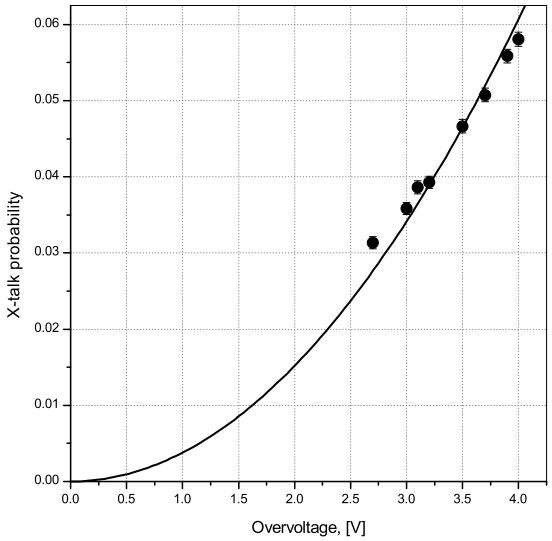

Fig. 19: The dependence of the cross-talk probability versus overvoltage at a fixed temperature (KETEK PM1125NS-SB0).

The full cross-talk probability was calculated with the Eq.(13). Then the p value was calculated with Eq.(15). The theoretical value of probability that only one cell is triggered by cross-talk event is given [7]: $p_{2phe}^{theory} = 4 \cdot p \cdot (1-p)^6$. On the other hand the experimental probability p_{2phe}^{exp} is the ratio of events number $N_{2p.e.}$ to the total number of events, where $N_{2p.e.} \approx N_{B_1}$. It was found that the ratio $p_{2phe}^{exp}/p_{2phe}^{theory}$ for Hamamatsu S10362-11-100C varies from 1 to 1.08 depending on a temperature and an overvoltage, and for Hamamatsu S13360-3050CS and KETEK PM1125NS-SB0 this ratio varies from 0.98 to 1.02. Thus it can be concluded that the model of four nearest neighbors works well for considered SiPMs.

5.4 Probabilities of after-pulses

In Fig.20, 22, the dependencies of the probabilities for after-pulses versus temperature are presented. This dependencies p_s and p_f at the current accuracy of the measurements are independent of a temperature. In Fig.21, 23, 28, 30 the dependencies of the probabilities for after-pulses versus overvoltage are presented. This dependencies were approximated with quadratic dependence on an overvoltage. In Fig.24, 25, 26, 27 the dependencies of time constants versus temperature and overvoltage are presented. The time constants τ_s and τ_f at a given measurement accuracy are independent on an overvoltage and temperature. In Fig.29 and Fig.31 the dependencies are not constant and we guess this happened because of systematic errors.

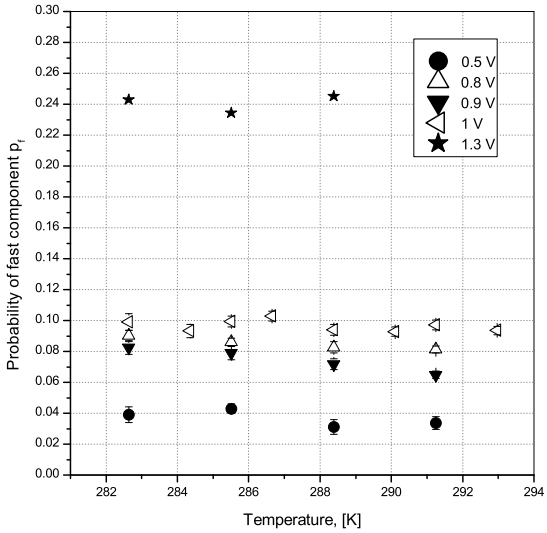

Fig. 20: The dependence of the fast component probability p_f for an after-pulse versus temperature at a fixed overvoltage (Hamamatsu S10362-11-100C).

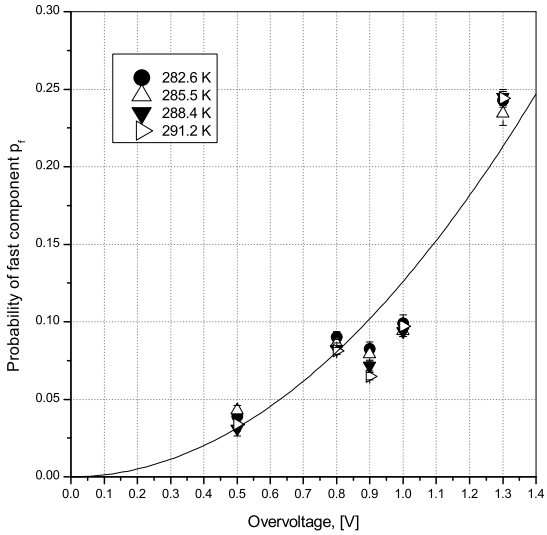

Fig. 21: The dependence of the fast component probability p_f for an after-pulse versus overvoltage at a fixed temperature (Hamamatsu S10362-11-100C).

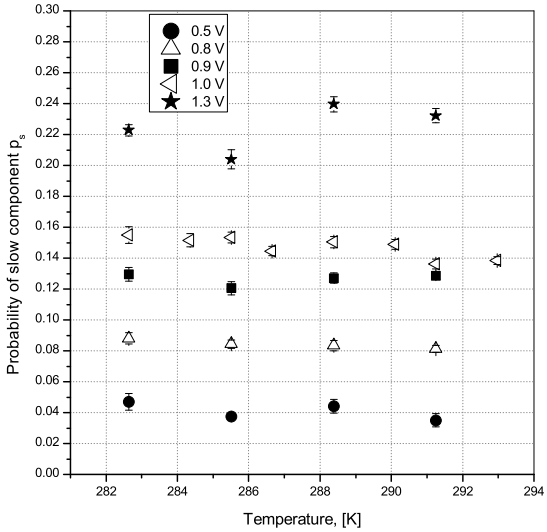

Fig. 22: The dependence of the slow component probability p_s for an after-pulse versus temperature at a fixed overvoltage (Hamamatsu S10362-11-100C).

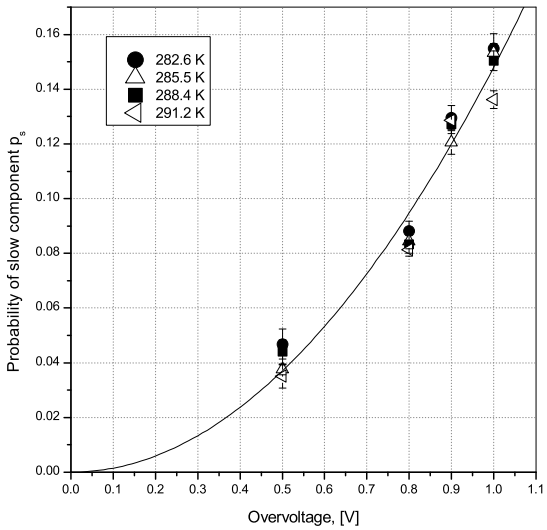

Fig. 23: The dependence of the slow component probability p_s for an after-pulse versus overvoltage at a fixed temperature (Hamamatsu S10362-11-100C).

6 Conclusions

In the work were present of measurement of dark noise rate, the probabilities for cross-talk and after-pulses and after-pulses time constants for three SiPMs types:

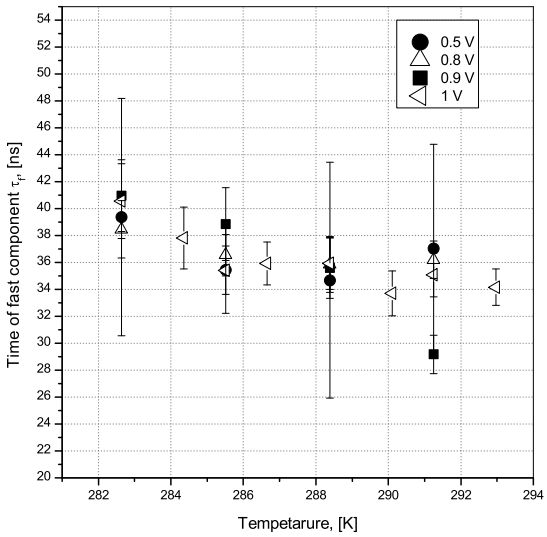

Fig. 24: The dependence of the fast time constant τ_f for an after-pulse versus temperature at a fixed overvoltage (Hamamatsu S10362-11-100C).

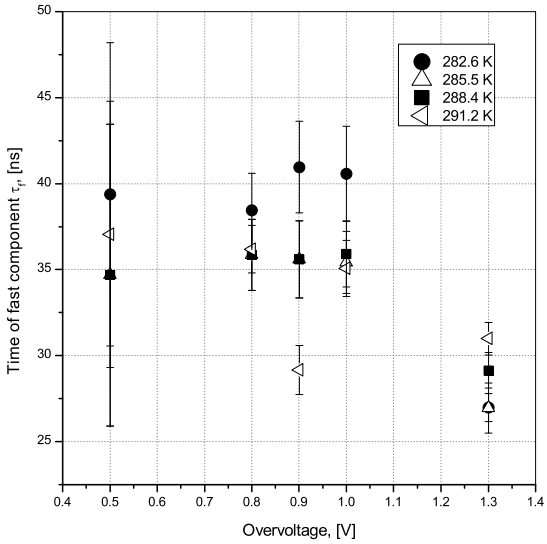

Fig. 25: The dependence of the fast time constant τ_f for an after-pulse versus overvoltage at a fixed temperature (Hamamatsu S10362-11-100C).

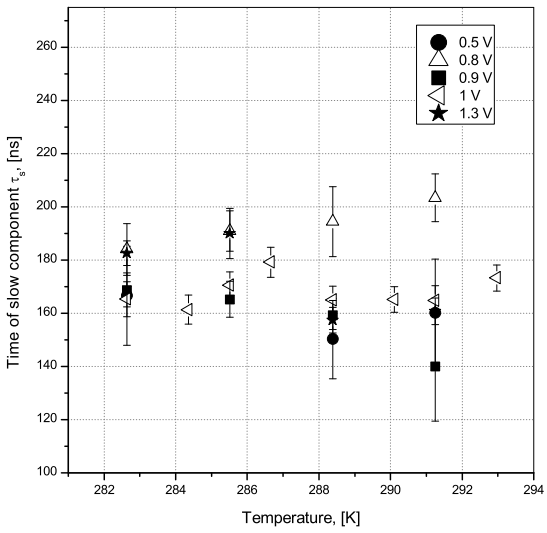

Fig. 26: The dependence of the slow time constant τ_s for an after-pulse versus temperature at a fixed overvoltage (Hamamatsu S10362-11-100C).

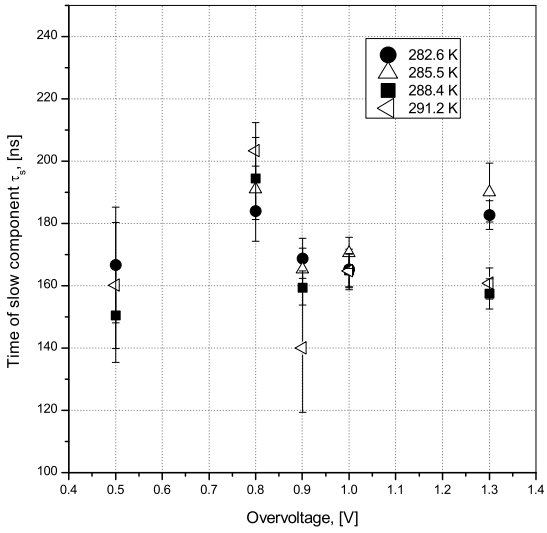

Fig. 27: The dependence of the slow time constant τ_s for an after-pulse versus overvoltage at a fixed temperature (Hamamatsu S10362-11-100C).

KETEK PM1125NS-SB0, Hamamatsu S10362-11-100C and Hamamatsu S13360-3050CS.

An offline signal processing was performed by the pulse approximation with reconstruction of amplitudes and start times to find these parameters. Besides the algorithm

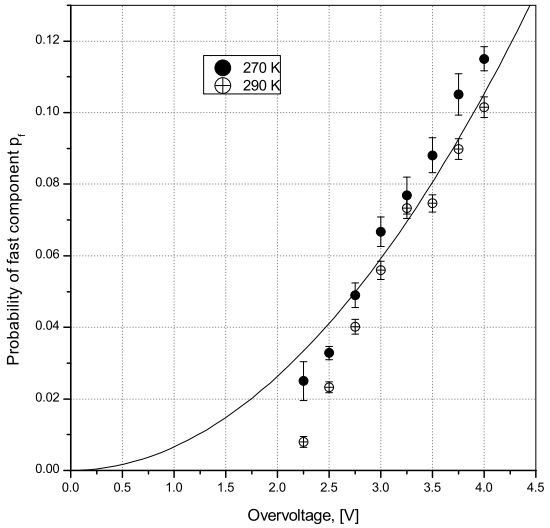

Fig. 28: The dependence of the fast component probability p_f for an after-pulse versus overvoltage at a fixed temperature (Hamamatsu S13360-3050CS).

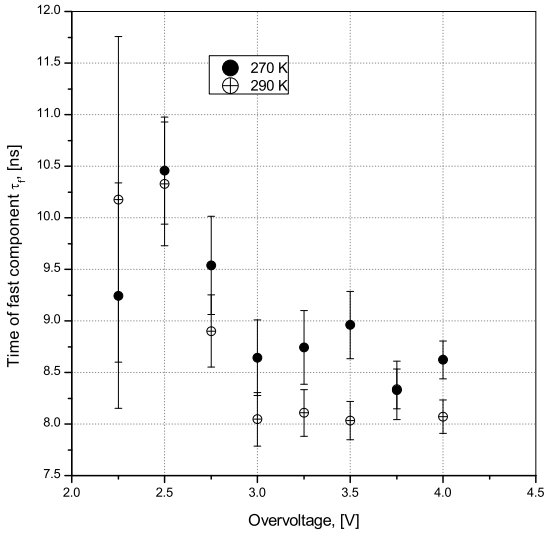

Fig. 29: The dependence of the fast time constant τ_f for an after-pulse versus overvoltage at a fixed temperature (Hamamatsu S13360-3050CS).

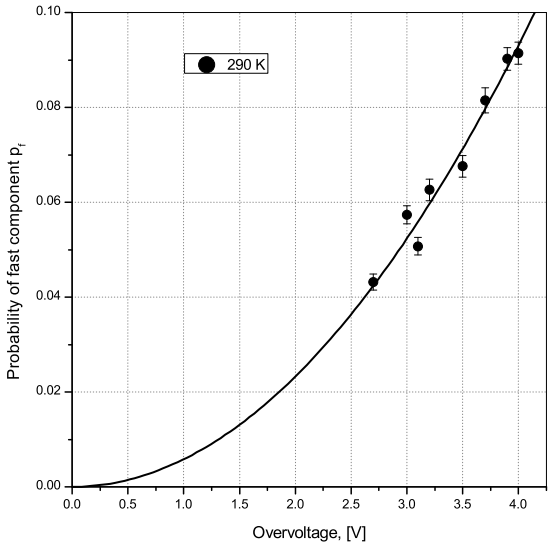

Fig. 30: The dependence of the fast component probability p_f for an after-pulse versus overvoltage at a fixed temperature (KETEK PM1125NS-SB0).

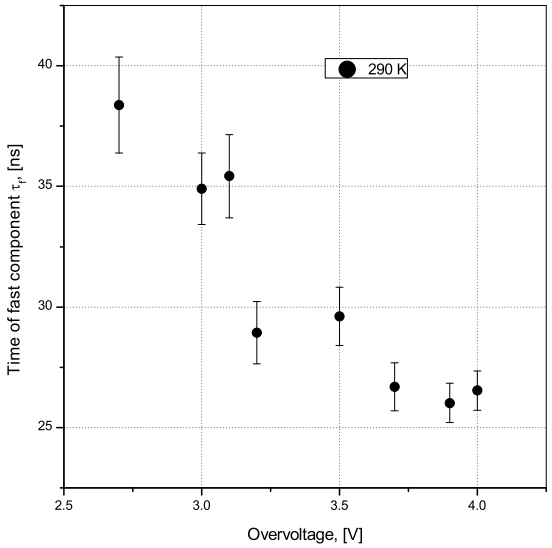

Fig. 31: The dependence of the fast time constant τ_f for an after-pulse versus overvoltage at a fixed temperature (KETEK PM1125NS-SB0).

used, there are three methods. The first - the measurement of the pulse rate depending on the amplitude threshold. The second - the integration a signal at a certain time interval and finding a number of events in the peaks. The third - the signal deconvolu-

tion and an approximation of the pulse interval spectrum. The first two methods are rather simple and can be used in an online analysis but they have a serious drawback - after-pulsing probabilities and after-pulsing time constants can't be found. The third method, and the method used in this study require large computing power, however, allow us to find after-pulsing parameters.

At achieved measurement accuracy in the temperature range from 0 to $20C^{\circ}$ the cross-talk probability, after-pulsing probabilities and after-pulsing time constants are independent on a temperature. SiPMs were checked for compliance with the four neighbors model. All three types of SiPMs have model discrepancy less than 10%.

The cross-talk probability for Hamamatsu S10362-11-100C at an operating overvoltage (1 V) is about 12%, for Hamamatsu S13360-3050CS and KETEK PM1125NS-SB0 (an operating overvoltage is 4 V) is about 6%. After-pulsing probabilities for Hamamatsu S10362-11-100C at an operating overvoltage is about 10% (fast component) и 15% (slow component). For Hamamatsu S13360-3050CS and KETEK PM1125NS-SB0 because of the small statistics it was studied only the fast component, which is about 10%. After-pulsing time constants for Hamamatsu S10362-11-100C are about 35 ns (fast component) and 170 ns (slow component), for Hamamatsu S13360-3050CS - 9 ns, for KETEK PM1125NS-SB0 - 28 ns. Dark noise rate for Hamamatsu S10362-11-100C at an operating overvoltage and 20 $^{\circ}C$ temperature is about 300 kHz/mm^2, for Hamamatsu S13360-3050CS - 30 kHz/mm^2, for KETEK PM1125NS-SB0 - 80 kHz/mm^2.

Thus, on the basis of the experiments we can conclude that Hamamatsu S13360-3050CS which has lower dark noise rate and the least after-pulsing time constants.

References

[1] E.A. Babichev et al., SiPM based photon counting detector for scanning digital radiography, JINST 10 (2015) C03002

[2] P. Dorosz et al., Silicon Photomultiplier's Gain Stabilization by Bias Correction for Compensation of the Temperature Fluctuations, , Nucl. Instrum. Meth. A 718 (2013) pp. 202–204

[3] N. Dinu et al., Temperature and Bias Voltage Dependence of the MPPC Detectors, IEEE Oct. 30 2010-Nov. 6 2010 pp.215 - 219

[4] Marco Ramilli, Characterization of SiPM: temperature dependencies, IEEE 19-25 Oct. 2008 pp. 2467 - 2470

[5] P.K. Lightfoot et al., Characterisation of a silicon photomultiplier device for applications in liquid argon based neutrino physics and dark matter searches, JINST 3 (2008) P10001

[6] Patrick Eckert et al., Characterisation Studies of Silicon Photomultipliers, Nucl. Instrum. Meth. A 620 (2010) pp. 217–226

[7] L. Gallego et al., Modeling crosstalk in silicon photomultipliers, Nucl. Instrum. Meth. A 787 (2015) pp. 153–156

[8] A. Vacheretc et al., Characterization and Simulation of the Response of Multi Pixel Photon Counters to Low Light Levels, Nucl. Instrum. Meth. A 656 (2011) pp. 69-83

[9] Y. Du et al., After-pulsing and cross-talk in multi-pixel photon counters, Nucl. Instr. and Meth. A 596 (2008) pp. 396-401

[10] Fabrice Retiere, Using MPPCs for T2K Fine Grain Detector, PoS PD07 (2006) 017

[11] J. Rosado et al., Modeling crosstalk and afterpulsing in silicon photomultipliers, Nucl. Instr. and Meth. A 787 (2015) pp. 153–156

[12] Daniel Orme et al., Measurement of PDE of MPPC with different wavelengths of light, PoS PD09 (2009) 019